

Cite this: *J. Mater. Chem. A*, 2015, **3**,  
11533

## Fast and reversible photo-responsive wettability on TiO<sub>2</sub> based hybrid surfaces†

Gwendoline Petroffe, Chao Wang, Xavier Sallenave, Gjergji Sini, Fabrice Goubard and Sébastien Peralta\*

A hybrid surface exhibiting a fast and reversible switch between hydrophobic and hydrophilic states was prepared by spin-coating a porous TiO<sub>2</sub> layer by a mixture of TiO<sub>2</sub> nanoparticles with 11-(4-phenylazo) phenoxy undecanoic acid (denoted as the AzoC11 acid). The nanocomposite film corresponding to the 10% AzoC11 acid/TiO<sub>2</sub> mass fraction exhibited both a very important and fast variation of the contact angle (by more than 120°), along with an excellent reversibility. The wettability switching is explained by the *trans* → *cis* → *trans* isomerization of the AzoC11 acid under light irradiation or heating. Upon *trans* → *cis* isomerization, optical absorption bands were found to exhibit drastic evolution, the origin of which is discussed in detail by means of a time-dependent density functional theory (TDDFT) study. Subsequent to these isomerization processes, various mechanisms explaining the wettability variations were investigated by comparing the results obtained by DFT calculations, wetting measurements for different surface ratios of the AzoC11 acid under UV irradiation, and by analyzing the molecular structure and molecular surfaces of *trans* and *cis*-isomers of the AzoC11 acid.

Received 6th March 2015  
Accepted 24th April 2015

DOI: 10.1039/c5ta01710f

www.rsc.org/MaterialsA

## Introduction

In recent years, superhydrophobic and superhydrophilic surfaces with a water contact angle greater than 150° and less than 10°, respectively, are of great scientific interest due to their potential applications in self-cleaning,<sup>1</sup> anti-fogging<sup>2</sup> or antireflective surfaces<sup>3</sup> and microfluid manipulations.<sup>4–6</sup> Furthermore, the rapid and reversible wetting transition between superhydrophilic and superhydrophobic states is one of the hot topics in research on developing functional materials in the last decade. Many investigations have shown that besides the chemical nature of surfaces, the roughness and morphology also affect their wetting behaviour.<sup>7,8</sup>

The reversible wetting variation can be induced by the surface energy variations or/and the morphology modifications. In general, external stimuli, such as temperature,<sup>9,10</sup> chemical treatment,<sup>11</sup> electrical potential,<sup>12</sup> pH<sup>13–17</sup> or light<sup>18</sup> can change the surface properties and the surface behavior. The use of materials with light-tunable wettability has promising applications notably because of avoiding the contact with materials which minimizes contaminations.

Laboratoire de Physicochimie des Polymères et des Interfaces (LPPI, EA 2528), Institut des Matériaux, Université de Cergy-Pontoise, 5 mail Gay-Lussac Neuville/Oise, 95000 Cergy-Pontoise Cedex, France. E-mail: sebastien.peralta@u-cergy.fr

† Electronic supplementary information (ESI) available: Theoretical absorption spectra of *trans*- and *cis*-AzoC11 acid in THF, absorption onset on the UV-vis spectra of AzoC11 acid solution, theoretical estimation of molecular-areas, expression of surface ratio, values of the wetting study, comparison of contact angle variations versus the irradiation conditions. See DOI: 10.1039/c5ta01710f

A wide number of inorganic materials are used for stimuli-responsive surfaces. Semiconductor oxides are well-known as stable, nontoxic and highly reactive materials which are able to induce a high wettability conversion between superhydrophobic and superhydrophilic states. In previous studies, surface wettability of light-responsive inorganic oxides under UV irradiation, such as ZnO,<sup>19</sup> TiO<sub>2</sub><sup>20–22</sup> or V<sub>2</sub>O<sub>5</sub><sup>23</sup> has been reported. However, the main problem with these materials is the too long time needed for the kinetic switching (several days for one cycle).<sup>22,24</sup>

As compared to inorganic materials, organic materials have many advantages in terms of the number of adaptable species, the potential for chemical modifications, and the reaction diversity. Such light-sensible materials are able to alter their properties reversibly, especially their wetting behaviour upon irradiation. These changes are often based on chromophoric groups of organic dyes such as azobenzene,<sup>4,25</sup> spiropyran,<sup>7,26</sup> coumarin<sup>27</sup> or cinnamate<sup>28</sup> which undergo a reversible isomerization under illumination. The wetting of azobenzene surfaces, for example, was tuned by alternation of UV and visible illumination for a few minutes.<sup>29</sup> Unfortunately, the water contact angle variations (CAV) are very small (10° for a smooth surface).<sup>29,30</sup> It is possible to increase the CAV using other solvents such as diiodomethane<sup>31</sup> or benzonitrile<sup>32</sup> instead of water.

Few authors have associated an organic layer with a semiconductor oxide. Cho *et al.* have elaborated a rough substrate based on layer-by-layer deposition of poly(allylamine hydrochloride) and SiO<sub>2</sub> nanoparticles.<sup>33</sup> This film was functionalized

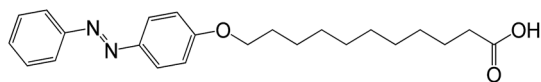


Fig. 1 11-(4-Phenylazo)phenoxy undecanoic acid (AzoC11 acid).

with a photoswitchable azobenzene molecule, the 7-[(trifluoromethoxyphenylazo)phenoxy]pentanoic acid (CF<sub>3</sub>AZO). This system can be switched between superhydrophobicity and superhydrophilicity with 20 min of UV irradiation and can be reversible within 3 h of visible light irradiation. Huang *et al.* have reported an original hybrid material based on a filter paper in cellulose pre-coated by a titanium ultrathin film.<sup>34</sup> With the CF<sub>3</sub>AZO monolayer self-assembled onto the titanium film, the water contact angle varied between 145.2° and 24.2° after 13 h of UV irradiation. The original high hydrophobicity was recovered after storage in the dark for one week. More recently, Wu *et al.* have presented a facile method of fabricating the surface with reversibly tunable wettability. A mixture of poly(styrene-butylacrylate-acrylic acid) with TiO<sub>2</sub> nanoparticles in tetrahydrofuran (THF) was cast onto the glass substrate.<sup>14</sup> The water contact angle of the film changed from the original 156° to about 0°, after irradiation with UV light for 2 h. The initial state was recovered after heating this superhydrophilic film at 150 °C for 1 h.

These three examples show the strong potential of hybrid materials to obtain significant variations in wetting. However, although the switching times are much faster compared to TiO<sub>2</sub> materials, they are too slow to be considered for use in the field of microfluidics.<sup>35</sup>

Aiming to prepare functional hybrid materials with both the advantages of inorganic nanoporous TiO<sub>2</sub> films and photosensitive moieties, we synthesized azobenzene functionalized titanium oxide derivatives with different degrees of coverage with azobenzene moieties. Initially, an organic photoswitchable molecule (Fig. 1), the 11-(4-phenylazo)phenoxy undecanoic acid (denoted as the AzoC11 acid) was easily synthesized. Then, the photosensitivity of the AzoC11 acid in both solution and deposited on a roughness controlled TiO<sub>2</sub> film was investigated. The azobenzene moieties of the AzoC11 acid/TiO<sub>2</sub> nanocomposite exhibited a reversible *trans* → *cis* isomerization transition upon irradiation with UV, leading to a change of surface wettability. Thanks to the combination of this chromophore with a controlled roughness of TiO<sub>2</sub>, a faster reversible wettability switch is obtained as compared to the previous studies in this domain.<sup>14,32,34</sup>

## Experimental section

### Materials

4-Phenylazophenol (98%), Triton X-100, acetyl acetone from Sigma-Aldrich, 11-bromoundecanoic acid (98%), potassium carbonate, titanium isopropoxide from Fisher Scientific, and poly ethylene glycol from Merck were all used as received. Titanium nanoparticles (TiO<sub>2</sub> P25) were provided from Degussa. Tetrahydrofuran (THF) was dried by distillation from sodium metal/benzophenone and stored over 4 Å molecular sieves.

Water used for the synthesis and contact angle measurements was purified by a Milli-Q system (resistance 18 MΩ).

### Techniques of analysis

<sup>1</sup>H and <sup>13</sup>C NMR spectra were recorded on a Bruker Avance DPX 250 MHz spectrometer. Chemical shifts are given in ppm using the residual solvent signal (CDCl<sub>3</sub>) as an internal reference. Fourier transform infrared (FTIR) spectra were recorded using a Bruker Tensor 27 spectrometer. The sample was pressed into KBr pellets. UV-visible measurements of the azobenzene derivative were performed at room temperature in spectrometric grade tetrahydrofuran solutions using a Jasco V570 spectrometer and an analysis cell with an optical path length of 10 mm.

Photoisomerizations *trans* → *cis* and *cis* → *trans* were realised from a UV lamp (15 W, λ<sub>max</sub> = 365 nm, intensity at 2.0 cm = 1.5 mW cm<sup>-2</sup>, Vilber Lourmat VL-215.LC) and blue light (150 W, λ<sub>max</sub> = 410 nm, intensity at 2.0 cm = 21.5 mW cm<sup>-2</sup>, Fort GLI 156), respectively. In all cases, the samples were placed at 2.0 cm.

The atomic force microscopy (AFM) experiments were performed in tapping mode with a Nanoscope V controller coupled with an Icon microscope from Bruker. Measurements were carried out in air at room temperature. For each sample, AFM images were recorded on at least four samples and in several places in order to check the reproducibility of the displayed images.

Contact angles (CA) were determined using a DSA10-Mk2 (Krüss, Germany) in air at room temperature with a 15 μL ultrapure water drop. The contact angles of the superhydrophilic surface are arbitrarily set at 10° because it is very difficult to obtain a reliable measurement of the superhydrophilic surface. For each sample, contact angles were measured on about three samples; five drops per sample were analyzed. The reported contact angle values correspond to the average of all measurements with an error bar corresponding to the standard deviation.

The molecular areas are estimated by extrapolation of the surface pressure isotherm obtained on a Langmuir trough (model 611 from Nima). The spreading solution was the AzoC11 acid dissolved in chloroform at a concentration of 0.4 mg mL<sup>-1</sup>. To obtain the molecular area of the *cis* form of the AzoC11 acid, the spreading solution was previously irradiated with UV light for 10 min. The monolayer was compressed with a barrier speed of 20 mm min<sup>-1</sup> and the subphase was the ultrapure water at 20 ± 1 °C. The molecular areas of the AzoC11 acid correspond to the average of 5 extrapolations of the surface pressure isotherm.

The layer thicknesses are the average of 10 measurements on two samples. The measurements are obtained by using profilometry (Dektak 150 from Veeco).

### Synthesis of 11-(4-phenylazo)phenoxy undecanoic acid (AzoC11 acid)<sup>36,37</sup>

To a solution of 4-phenylazophenol (1.12 g, 5.6 mmol) and 11-bromoundecanoic acid (3 g, 11.2 mmol) in 150 mL of absolute ethanol was added dry potassium carbonate (1.58 g, 16.8 mmol). The mixture was stirred under reflux for 48 h. After cooling, the ethanol was evaporated and the residue was

dissolved in chloroform (200 mL). The organic layer was washed with HCl (2 M) solution ( $2 \times 50$  mL), then water ( $3 \times 50$  mL), dried over  $\text{MgSO}_4$  and concentrated. The product was purified by recrystallization from acetonitrile to give an orange solid (1.15 g, 54%).  $^1\text{H}$  NMR ( $\text{CDCl}_3$ )  $\delta$  = 7.94–7.87 (m, 4H, *Ar*-N=), 7.54–7.43 (m, 3H, *Ar*), 7.01 (dd,  $J$  = 6.9 Hz et  $J$  = 2.1 Hz, 2H, *Ar*-O), 4.04 (t,  $J$  = 6.5 Hz, 2H,  $\text{CH}_2\text{O}$ ), 2.30 (t,  $J$  = 7.3 Hz, 2H,  $\text{CH}_2\text{CO}$ ), 1.85–1.76 (m, 2H,  $\text{CH}_2\text{CH}_2\text{O}$ ), 1.67–1.61 (m, 2H,  $\text{CH}_2\text{CH}_2\text{CO}$ ), 1.50–1.42 (m, 2H,  $\text{CH}_2\text{CH}_2\text{CH}_2\text{O}$ ), 1.31 (m, 10H,  $\text{CH}_2$ ).  $^{13}\text{C}$  NMR ( $\text{CDCl}_3$ )  $\delta$  = 179.2, 161.8, 152.6, 146.7, 130.3, 129.0, 124.9, 122.5, 114.7, 68.4, 34.4, 33.9, 29.4, 29.3, 29.2, 29.1, 29.0, 26.0, 24.6. IR ( $\text{cm}^{-1}$ ): 2936, 2921, 2849, 1709, 1606, 1586, 1499, 1479, 1435, 1309, 1281, 1249, 1221, 1146, 1019, 845. Anal. calcd for  $\text{C}_{23}\text{H}_{30}\text{N}_2\text{O}_3$ : C, 71.94; H, 7.90; N, 7.34. Found: C, 72.22; H, 7.91; N, 7.32.

### Preparation of substrates

The substrates are composed of a glass slide with a coating of a dense and nanoporous  $\text{TiO}_2$  film.<sup>38</sup> All microscope slides from RS France were subsequently cleaned in a beaker of dilute Hellmanex solution (5%) at least for 30 min at 50 °C, rinsed with ultrapure water, sonicated for 10 min in ethanol, before being treated for 10 min by UV-ozone treatment (UVO cleaner 42 Jeligh). The glass substrates were used immediately.

A dense layer of  $\text{TiO}_2$  is applied by spin coating from a precursor of  $\text{TiO}_2$  solution. For the preparation of the solution of the  $\text{TiO}_2$  precursor, 7 drops of nitric acid (70% v/v) and 500  $\mu\text{L}$  of water were added to 20 mL of pure ethanol. The solution was stirred for 30 min. 1.5 mL of titanium isopropoxide was added to this solution. The solution was mixed and kept for 24 h without light. The  $\text{TiO}_2$  solution was deposited by spin-coating on the microscope slides at 3000  $\text{tr min}^{-1}$  for 60 s. The layers were then annealed at 500 °C for 15 min. The thickness measured by using the profilometer was about 80 nm.

A nanoporous layer of  $\text{TiO}_2$  is applied by spin coating with a  $\text{TiO}_2$  paste. For the preparation of the  $\text{TiO}_2$  paste, 100 mg of  $\text{TiO}_2$  nanoparticles was dispersed in 10 mL of ultrapure water by sonication for 10 min. 100  $\mu\text{L}$  of acetyl acetone, 120  $\mu\text{L}$  of acetic acid and 100  $\mu\text{L}$  of Triton X-100 were added. The mixture was vigorously stirred to get a colloidal state. 120 mg of poly ethylene glycol (PEG,  $M_w = 4000$   $\text{g mol}^{-1}$ ) was employed as the blowing agent. With magnetic bar stirring, this colloidal  $\text{TiO}_2$  was thoroughly mixed for 24 h followed by spin coating deposition on the microscope slides covered with the dense  $\text{TiO}_2$  layer at 2800  $\text{tr min}^{-1}$  for 40 s. Finally, the substrate was gradually annealed at

550 °C, for over 30 min. A 1000 nm thick film was obtained, as measured by using a profilometer. These titanium layers allow roughness to be induced on the substrates and promote adhesion of the active layer during the spin coating.

### Preparation of AzoC11 acid/ $\text{TiO}_2$ nanocomposite films

The nanocomposite film is composed of a mixture of the AzoC11 acid and  $\text{TiO}_2$  nanoparticles (P25) in THF. 100 mg of  $\text{TiO}_2$  nanoparticles were dispersed in 2 mL of THF by sonication for 10 min. 5, 8, 10, 15 or 25 mg of AzoC11 acid was added to this mixture. The solution was denoted as  $x\%$  AzoC11 acid/ $\text{TiO}_2$ . After 24 h of vigorous stirring, the mixture was a uniform milky liquid, slightly orange in colour. The AzoC11 acid/ $\text{TiO}_2$  solutions were spin coated on the substrates at 2800  $\text{tr min}^{-1}$  for 40 s. Visually, the samples which are initially whitish become slightly orange. This nanocomposite film provides easily a structured surface.

### Computational methodology

DFT<sup>39</sup> calculations employing the B3LYP<sup>40,41</sup> and  $\omega\text{B97XD}$ <sup>42</sup> functionals were performed with a Gaussian 09 program.<sup>43</sup> The geometry optimizations for all the molecules were carried out without symmetry constraints and were followed by frequency calculations. Given that several properties of this compound depend principally on the pi-conjugated backbone, a limited alkyl chain without the carboxylic group was considered for the calculation of the optical properties and for the solvation energy of the *cis*-isomer. The spectroscopic properties of the molecules were calculated by mean of a time dependent density functional theory method (TDDFT)<sup>44–48</sup> with the 6-31G(d) basis set. Up to 20 excited states were calculated and the theoretical absorption bands were obtained by considering a band half-width at half-maximum of 0.2 eV.<sup>49</sup> The interaction energies of the model water-complexes were calculated with respect to the isolated molecules at the  $\omega\text{B97XD}/6\text{-311+G(d)}$  level in gas phase, and were corrected for the basis set superposition error (BSSE) by the counterpoise correction method of Boys and Bernardi.<sup>50</sup> The zero point energy (ZPE) corrections were also taken into account.

## Results and discussion

### Geometry and molecular orbitals (MO) of *trans*- and *cis*-isomers

The geometrical differences between the two isomers *trans*- and *cis*-AzoC11 acid are shown in Fig. 2. While the *trans*-isomer

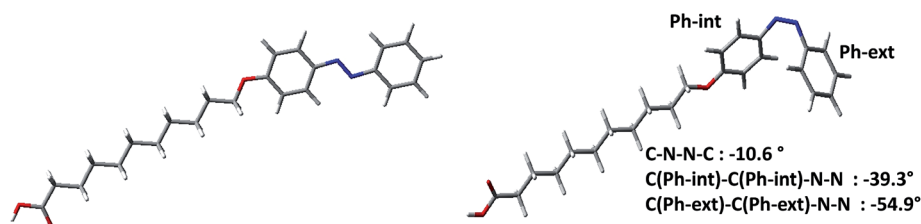


Fig. 2 Geometries of the *trans*- and *cis*-azoC11 acid as optimized at the B3LYP/6-31G\* level by taking into account the solvent effect (THF). Some dihedral angles around the N=N bond in the *cis*-azoC11 acid are given.

exhibits a perfectly planar  $\pi$ -system backbone, a C–N=N–C dihedral angle of  $-10.6^\circ$  is found in the case of the *cis*-isomer, due to the steric hindrance between the phenyl rings.

Inspection of Fig. 3 indicates two important differences between *trans*- and *cis* MOs: (i) increase of the  $n$ - $\pi$  mixture appears in the MO plots from HOMO–1 to HOMO in the case of the *cis*-isomer and (ii) due to the non-zero C–N=N–C dihedral angle ( $-10.6^\circ$ ) in the *cis* isomer, the  $\pi$ -conjugation efficiency decreases upon *trans*  $\rightarrow$  *cis* isomerization. The energy order between the  $\pi$ -type (HOMO) and the  $n$ -type (HOMO–1) orbitals in the *trans*-isomer is reversed in the case of the *cis*-isomer (dominant  $n$ -character in HOMO, dominant  $\pi$ -character in HOMO–1), which will be seen to impact the positioning and intensity of the absorption spectra. As for the LUMOs, they remain dominantly of N=N  $\pi$ -contribution for both isomers.

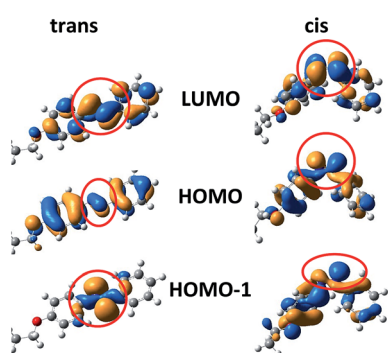


Fig. 3 Selected set of MO plots corresponding to the *trans*- and *cis*-azoC11 acid. The alkyl chains are hidden for the sake of clarity. The encircled parts (red circles) in each MO correspond to the contribution of the N–N fragment.

### Absorption spectra of *trans*- and *cis* isomers in solution

The experimental UV-vis spectra of the AzoC11 acid in THF, before and after 40 s of UV irradiation, are given in Fig. 4a, whereas the corresponding theoretical absorption spectra of the *trans*- and *cis*-AzoC11 acid in THF are given in Fig. 4b. Both *trans*- and *cis*-AzoC11 acid spectra present one low-energy band centered around 450 nm, and a higher-energy one peaking around 320 nm. Theoretical absorption spectra indicate that each band is due to a single excitation (Fig. S1a of the ESI<sup>†</sup>), principally of the  $n \rightarrow \pi^*$  and  $\pi \rightarrow \pi^*$  character for the low- and high energy bands respectively (Fig. 4b). In the case of the *trans*-isomer, the theoretical  $n \rightarrow \pi^*$  transition (HOMO–1  $\rightarrow$  LUMO) is symmetry forbidden (zero oscillator strength, Fig. 4b), due to the zero-overlap of the corresponding MOs (Fig. 3). The non-zero experimental value for this band may be due to the geometrical deformations of the *trans*-isomer in solution, which are absent in the theoretical results. Indeed, test calculations considering small deviations from the planarity around the N=N bond ( $2^\circ$ ,  $5^\circ$ ,  $8^\circ$ , and  $10^\circ$ ) result in a nonzero oscillator strength of 0.002, 0.003, 0.022, and 0.033 respectively for the  $n \rightarrow \pi^*$  transition (Fig. S1b of the ESI<sup>†</sup>).

Upon UV-irradiation of the *trans*-isomer, the intensity of the  $\pi$ - $\pi^*$  transition band ( $\sim 350$  nm) decreases significantly and the maximum position is blue shifted to 315 nm. These important modifications are principally due to two effects: (i) because of the  $n$ - $\pi$  nature mismatch between HOMO–1 and LUMO at the N=N moiety of the *cis*-isomer, the HOMO–1–LUMO overlap (impacting the transition intensity) is reduced significantly, and (ii) in the case of the *cis*-isomer, the  $\pi$ - $\pi^*$  excitation principally corresponds to the HOMO–1  $\rightarrow$  LUMO transition (77%), involving a larger gap as compared to the HOMO–LUMO gap for

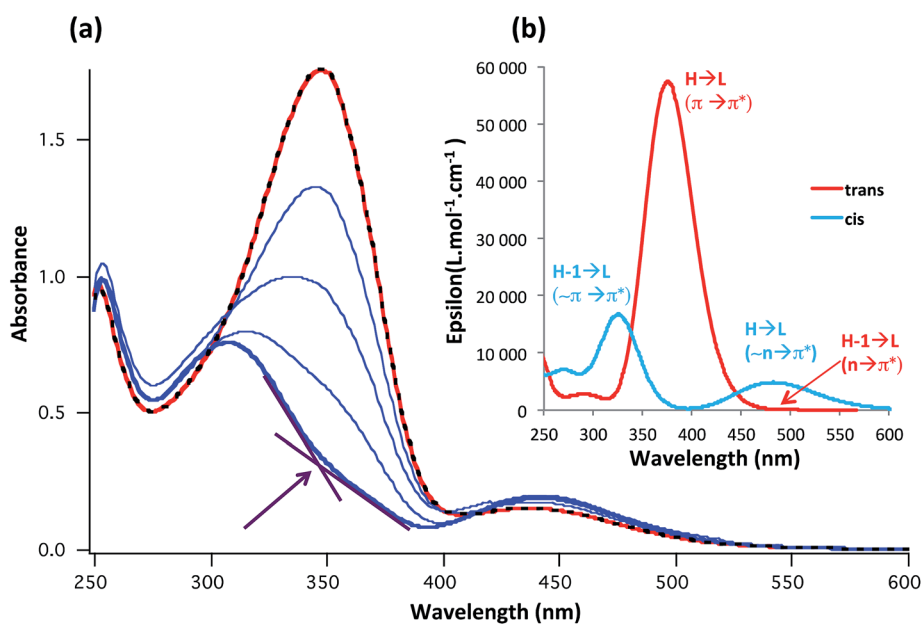


Fig. 4 (a) UV-vis spectra of the AzoC11 acid in THF solution ( $C = 10^{-4}$  mol L $^{-1}$ ) before (red curve), during (blue curve) and after (blue bold curve) UV irradiation and after the blue irradiation (black dotted curve). The highlighted discontinuity of the high-energy band of the *cis*-isomer is supposed to be due to the presence of some *trans*-isomer. Inset (b) theoretical absorption spectra obtained at the TDB3LYP/6-31G\* level. The dominant transitions are also indicated for each band.

the *trans*-isomer, consequently resulting in the observed blue-shift. Similar arguments apply to the  $n-\pi^*$  transition band at 442 nm: due to the  $n-\pi$  mixing, the  $n-\pi^*$  transition in the case of the *cis*-isomer becomes less forbidden, resulting in a slight increase in the intensity of the low-energy band. Upon *trans*  $\rightarrow$  *cis* isomerisation of the AzoC11 acid in THF solution, the absorption spectra exhibit important changes in the intensity and position of the bands. The UV-vis spectroscopy presents consequently an easy method to follow the *trans*  $\rightarrow$  *cis* isomerization.

The experimental UV-vis spectra of the AzoC11 acid in THF during UV irradiation (Fig. 4a) suggest that some amount of the *trans*-isomer is still present in solution. Indeed, after 40 s of UV irradiation (blue bold curve), the high-energy band exhibits a discontinuity of the right-hand part (highlighted by an arrow, Fig. 4a), the position of which fits perfectly with the maximum position of the *trans*-isomer. This conclusion is supported by the similar positions of the absorption onset (Fig. S2 of the ESI†) between the two bands in the experimental spectra, both features (discontinuity and identical onset) being absent in the theoretical absorption spectra (Fig. 4b). A possible explanation for this mixture could be given in terms of the relative stability of the *trans*- and *cis*-isomers, the latter one being  $\sim 11$  kcal mol $^{-1}$  higher in energy as compared to the *trans*-isomer ( $\omega$ B97XD/6-311+G\*\* level in THF). Finally, after subsequent blue

illumination, *cis*  $\rightarrow$  *trans* isomerisation occurs with very high yield, as the spectrum of the *trans*-azobenzene is totally restituted. The restituted spectrum (black dotted line) is superposed on the initial spectrum (red solid line) in Fig. 4a.

Despite the presence of some mixture of *cis*- and *trans*-isomers in solution, Fig. 4a indicates that the intensity of the high-energy absorption band of the AzoC11 acid upon UV and visible light irradiation exhibits important variations and is almost totally reversible. Fig. 5 shows the normalized absorption intensities of the high-energy band of the AzoC11-acid for several UV  $\leftrightarrow$  vis irradiation cycles.

The absorption maxima and minima at 348 nm correspond respectively to predominantly the *trans*- and *cis*-AzoC11 acid. The *trans*  $\rightarrow$  *cis* and *cis*  $\rightarrow$  *trans* isomerization of a solution of the AzoC11 acid is fast (less than 4 min for a full cycle) and completely reversible, making the AzoC11 acid a good candidate for developing photosensitive surfaces.

### Morphology characterization of nanocomposite films

The nanocomposite film is composed of a mixture of the AzoC11 acid and TiO $_2$  nanoparticles (P25) in THF spin coated on the titanium substrate. Optimization of a large and reproducible photoresponsive switch is based on the control of wettability of the film, which is generally influenced by the morphology and surface free energy. The former is often exhibited as the surface roughness, and the latter is usually displayed as the change in the dipole moment.

Firstly, the roughness of the film was estimated from AFM height images before and after the AzoC11 acid/TiO $_2$  deposition (Fig. 6).

The AFM images of the substrate reveal the nanoporous structure of the TiO $_2$  layer. The pores are formed by calcination of the blowing agent (PEG,  $M_w = 4000$  g mol $^{-1}$ ). The average size of grains is 300 nm. These grains are therefore the result of the aggregation of nanoparticles whose initial diameter is 20 nm. The images of the pure TiO $_2$  film and the AzoC11 acid/TiO $_2$  layer are very similar. However the slight orange color of the sample shows that the organic layer is present. No additional aggregates were observed between the image in Fig. 6(a) and the image in Fig. 6(b), and the AzoC11 acid forms a homogeneous

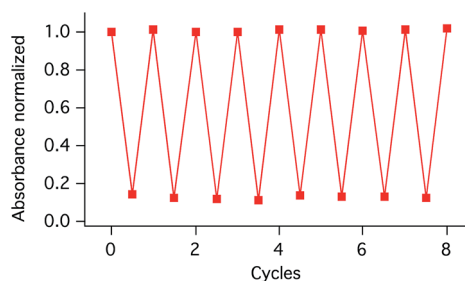


Fig. 5 Reversible *trans*-*cis* isomerisation of the AzoC11 acid in THF ( $C = 5 \times 10^{-5}$  mol L $^{-1}$ ) under 2 min UV irradiation and 2 min blue light irradiation. The location of the markers indicate the normalized absorbance of the high-energy absorption band (at 348 nm) of the AzoC11 acid upon UV and visible light irradiation.

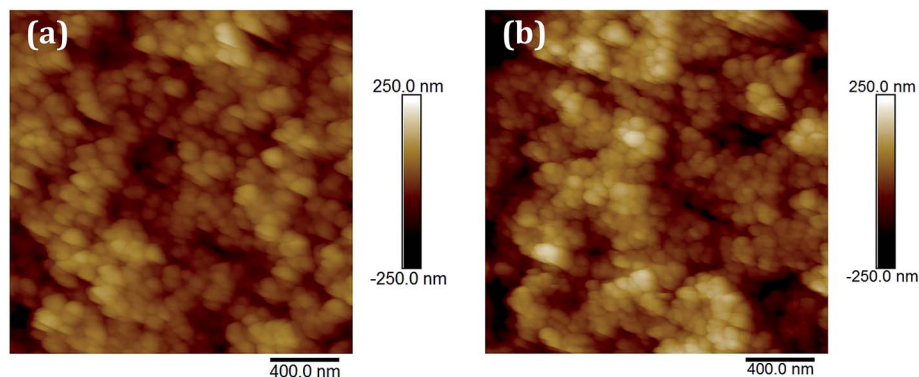


Fig. 6 AFM images of the substrate: dense + nanoporous TiO $_2$  layers (a) and the mixture of 10% wt AzoC11 acid/TiO $_2$  on dense + nanoporous TiO $_2$  layers (b) ( $2 \mu\text{m} \times 2 \mu\text{m}$ ).

layer on the surface. The active layer thus preserves the nanoporous nature of the substrate. Furthermore, the AzoC11 acid appears to form a homogeneous layer on the nanoparticle surface without filling the nanopores. Indeed, the root-mean-square roughness ( $R_{\text{rms}}$ ) calculated on 5 images of  $4 \mu\text{m}^2$  were very close, respectively  $49 \pm 4 \text{ nm}$  and  $64 \pm 3 \text{ nm}$  for pure  $\text{TiO}_2$  and the AzoC11 acid/ $\text{TiO}_2$  layer on the substrate.

### AzoC11-acid/ $\text{TiO}_2$ nanocomposite films: effect of surface-coverage on the contact angles

**Surface coverage ratios.** The wettability of the nanocomposite films on nanoporous  $\text{TiO}_2$  layers is followed by measuring the contact angle. The influence of surface-coverage on the contact angles was studied by considering the AzoC11-acid/ $\text{TiO}_2$  weight ratios of 0, 5, 8, 10, 15 and 25%. In order to correlate these weight ratios with the individual surface ratios of the *trans*- and *cis*-AzoC11 acid on the  $\text{TiO}_2$  nanoparticles, the molecular areas of the *trans*- and *cis*-AzoC11 acid were estimated by extrapolating surface pressure isotherms. The molecular areas of  $0.27 \pm 0.02 \text{ nm}^2$  and  $0.39 \pm 0.08 \text{ nm}^2$  for the *trans*- and *cis*-isomers respectively were found, and the results were also supported by the theoretical estimations of  $0.26 \text{ nm}^2$  and  $0.41\text{--}0.42 \text{ nm}^2$  (see the ESI: annexe III†). The value of the *trans* AzoC11 acid is comforted by the molecular area of the *trans* 4-octyl-[phenylazo-phenoxy] pentanoic acid estimated by Zhang ( $0.28 \text{ nm}^2$ ).<sup>51</sup>

Based on these molecular areas and the specific area of  $\text{TiO}_2$  nanoparticles P25 ( $55 \text{ m}^2 \text{ g}^{-1}$ ), the surface ratio of the AzoC11 acid on the nanoparticles can be estimated (see the ESI: annexe IV†). The surface ratios for the different mass fractions of the AzoC11 acid are presented in Table 1.

Note that an AzoC11 acid/ $\text{TiO}_2$  weight ratio of  $\sim 10\%$  seems to correspond to roughly 111% of  $\text{TiO}_2$  surface coverage with the *cis*-AzoC11 acid, but only 77% with the *trans*-AzoC11 acid.

**Effect of surface-coverage on the contact angles.** In the following, unless otherwise specified, the surface coverage ratios considered during the discussions will correspond to the surface ratios of the *trans*-AzoC11 acid (Table 1). The contact angles, corresponding to nanocomposite films with different AzoC11 acid/ $\text{TiO}_2$  surface ratios, were measured and shown in Fig. 7a.

**Initial contact angles (ICA).** In the absence of the AzoC11 acid, the  $\text{TiO}_2$  surface is superhydrophilic (the contact angle is less than  $10^\circ$ ). Fig. 7a suggests clearly that the increase of the ICA with increasing surface ratios between 0 and 193% is simply due to the increase in surface coverage with the AzoC11 acid (Table 1). The ICA increase rapidly when the AzoC11/ $\text{TiO}_2$  surface ratio is smaller than 62%, but remain stable (close to  $150^\circ$ ) for larger surface coverage values. Modulating a surface state from a superhydrophilic to a superhydrophobic state can thus be easily achieved by varying the amount of the AzoC11 acid in the mixture.

**Contact angles after UV irradiation.** Contact angles after UV irradiation (CAAUV) are lower than the initial contact angles for all surface ratios,<sup>53</sup> which could be explained by a competition between different processes: (i) *trans*  $\rightarrow$  *cis* isomerization of the azobenzene function upon UV irradiation induces a variation in the dipole moment, which has been considered as the dominant factor influencing the surface energy upon isomerization.<sup>54,55</sup> Indeed, the theoretical dipole moments of the isolated *trans*- and *cis*-AzoC11 acid ranges are, respectively, from 2.2–2.9 D and 3.6–6.1 D (B3LYP/6-31G\*\* level “in THF”). While the

Table 1 Surface ratios (in %) calculated as a function of the mass fraction of the AzoC11 acid

Mass fraction of AzoC11 acid/ $\text{TiO}_2$	5%	8%	10%	15%	25%
Surface ratios with <i>trans</i> AzoC11 acid	$39 \pm 3\%$	$62 \pm 5\%$	$77 \pm 6\%$	$116 \pm 9\%$	$193 \pm 14\%$ (ref. 52)
Surface ratios with <i>cis</i> AzoC11 acid	$56 \pm 12\%$	$89 \pm 19\%$	$111 \pm 23\%$	$167 \pm 34\%$	$279 \pm 57\%$

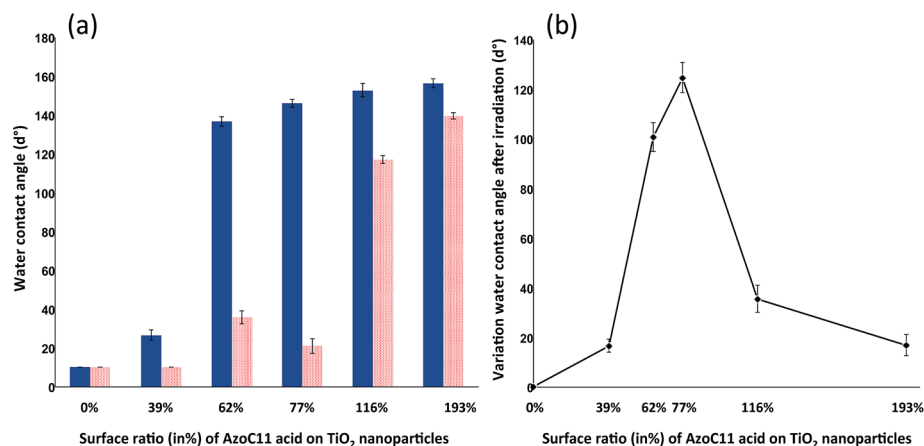


Fig. 7 (a) Initial water contact-angle for different surface ratios of the AzoC11 acid (full blue bars), and contact angle after 12 min of UV irradiation (patterned red bars). (b) The variations of the contact angles between before and after the UV irradiation are shown by the diamond markers ( $\blacklozenge$ ). The authors recall that the angles of superhydrophilic surfaces are arbitrarily set at  $10^\circ$ .

absolute values of the dipole moments of the AzoC11 acid on the TiO<sub>2</sub> surface may be different as compared to the isolated molecules, their trend between *trans*- and *cis*-isomers is expected to remain identical. The polarity of the AzoC11 acid thus increases after UV irradiation, in turn increasing the surface hydrophilicity and decreasing the contact angle. (ii) *Trans* → *cis* isomerization additionally allows for the establishment of hydrogen bonds between the nitrogen lone pairs and water molecules, thus increasing the surface hydrophilicity. Indeed, the HOMO plot of the *cis*-isomer (Fig. 8a) shows both nitrogen lone pairs oriented outside with respect to the surface. Our test calculations on the model *cis*-AzoC11 acid–2H<sub>2</sub>O complex clearly indicate the establishment of efficient hydrogen bonds, with a net energy stabilization of 5.4 kcal mol<sup>-1</sup>, consistent with a typical value of ~3 kcal mol<sup>-1</sup> per individual H-bond. In contrast, the nitrogen lone pairs are little visible when the AzoC11 acid is in the *trans* form, as also suggested by the shape of HOMO–1 (Fig. 3). (iii) Upon UV irradiation, photogenerated holes diffuse to the TiO<sub>2</sub> surface and react with lattice oxygen of TiO<sub>2</sub> itself, resulting in the creation of oxygen vacancies at the surface.<sup>56</sup> These oxygen vacancies are presumably favorable for water adsorption.<sup>57</sup> Water molecules are both adsorbed on defect sites and dissociated, resulting in the generation of two hydroxyl groups on each defect<sup>20,34,58</sup> (Fig. 8b). Increased hydrophilicity character of the TiO<sub>2</sub> (and global) surface will consequently occur.

The change in the contact angles after UV irradiation can thus result from a competition between these three factors. However, hydrophobicity-to-hydrophilicity switching times are much larger for the pristine titania surface as compared to the TiO<sub>2</sub> surface covered with the AzoC11 acid, suggesting that the third factor should be of minor influence in the above competition. This conclusion is also supported by the observation that decreasing the free surface of TiO<sub>2</sub> by increasing the surface coverage with the AzoC11 acid, results in an increased contact angle variation (Fig. 8b).

Concerning the evolution of the CAAUV with the increasing surface ratio (Fig. 7b), the smallest CAAUV corresponds to the pristine TiO<sub>2</sub> surface (0% surface ratio, Fig. 8a). The increase in

CAAUV in the presence of the AzoC11 acid can be due to the fact that the *trans* → *cis* isomerization is not complete even after 40 min of UV irradiation (Fig. 4). The CAAUV remains however less than 40° for surface ratios from zero to 77%, which is consistent with both the 77% of the surface coverage ratio for the *trans*-isomer and the 111% of the surface coverage ratio for the *cis*-isomer. Indeed, due to important geometrical modifications during the *trans* → *cis* isomerization (increase in the molecular areas from 0.27 nm<sup>2</sup> to 0.39 nm<sup>2</sup>), free room is needed around the *trans*-azobenzene moieties.<sup>59</sup> The 77% surface ratio for the *trans*-isomer (10% of weight ratio) thus corresponds to enough free room around the *trans*-azobenzene groups for the *trans* → *cis* isomerization to be sterically unhindered. As expected, the CAAUV rises dramatically when the surface ratio for the *trans*-isomer is greater at 100%, suggesting a small degree of *trans* → *cis* isomerisation. This last effect is consistent with the insufficient free space around *trans*-azobenzene groups for a sterically unhindered *trans* → *cis* isomerization.

**Contact angle variations.** The contact angle variations (calculated as ICA-CAAUV, Fig. 7b) depend consequently on the composition of the AzoC11 acid/TiO<sub>2</sub> mixture. In line with the evolution of ICA and CAAUV, the contact angle variations initially increase due to the sharp increase in ICA whereas CAAUV remains small due to efficient *trans* → *cis* isomerization. The contact angle variation (ICA-CAAUV) reaches the maximum value of 124.5° when the AzoC11 acid/TiO<sub>2</sub> mass ratio reaches 10%, which corresponds to the ideal value of roughly 100% for the surface ratio (coverage) with the *cis*-isomer. For surface ratios larger than this ideal value, the *trans*-AzoC11 acid layer becomes very compact and the ICA continues to remain large, but the azobenzene groups are less and less able to undergo *trans* → *cis* isomerization because of the increased steric hindrance, thus resulting in much larger CAAUV and smaller contact angle variation.

These results show that there is a good correlation between the variations of the contact angle and the AzoC11 acid/TiO<sub>2</sub> surface ratios. The mixture at 10% wt of the AzoC11 acid, resulting in *trans*- and *cis*-surface ratios of roughly 77% and 111% respectively, is a good compromise between the amount

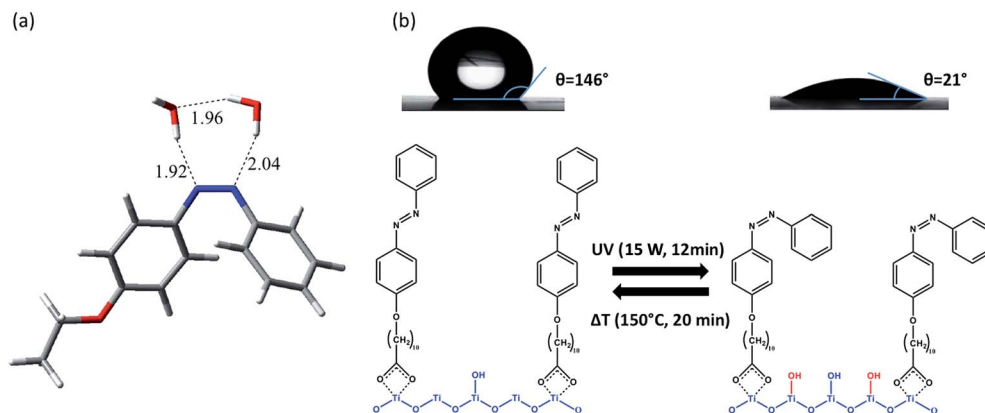


Fig. 8 (a) Model *cis*-AzoC11 acid–2H<sub>2</sub>O complex as calculated at the wB97XD/6-311+G(d,p) level by taking into account the effect of the solvent (water). The indicated distances are in Å. (b) The different effects of UV irradiation on AzoC11 acid/TiO<sub>2</sub>: azobenzene isomerization and hydroxyl photo-generation (in red).

of the AzoC11 acid present at the surface of TiO<sub>2</sub> and its ability to isomerize. In addition, for this fraction, the contact angle variation is very important and fast: over 124° after 12 min under UV irradiation.

### Reversibility study

Fig. 9 shows the evolution of water contact angles of the 10% wt AzoC11 acid/TiO<sub>2</sub> film as a function of irradiation time under UV light (15 W,  $\lambda_{\text{max}} = 365$  nm) and heating at 150 °C to induce a return to the hydrophobic state.<sup>60</sup>

Upon UV irradiation, the azobenzene-groups in the film isomerize from the *trans*- to the *cis*-conformation, resulting in a decrease in the contact-angle and film switching from the superhydrophobic to superhydrophilic state. Subsequent heating of AzoC11 TiO<sub>2</sub> films induces reverse *cis* → *trans* isomerization, and the film hydrophobicity is accordingly recovered. The minimum of contact angle is obtained after 12 min of UV irradiation. After 20 min at 150 °C, the contact angle recovers almost its initial value. The variation state is reversible and the full cycle is only for 32 min. This is to our knowledge, both the most rapid kinetics encountered in the literature and with large variation as well.

The reversibility of the photoresponsive switch was estimated by following the evolution of the water contact angle of the 10% wt AzoC11 acid/TiO<sub>2</sub> film during several cycles (Fig. 10). Each cycle corresponds to 12 min of UV irradiation followed by 20 min of heating at 150 °C.

The water contact angle of the 10% wt AzoC11 acid/TiO<sub>2</sub> film decreased from 144° to 16° after 12 min of UV irradiation. The quasi original high hydrophobicity was recovered after heating the sample at 150 °C for 20 min. The process of reversible switching of the surface wettability was carried out over 3 cycles of UV irradiation and heating which indicates that the film has reproducible reversible wettability. While the contact angle after the first cycle is less than the initial contact angle (118° and 144° respectively), it remains however constant for the next cycles.

Different hypotheses can be proposed to explain the difference between the initial contact angle and the contact angle after the first cycle. The first hypothesis is based on the partial reversibility of *cis* → *trans* isomerization. Unlike in solution, the mobility of AzoC11 acids is limited. When AzoC11 acids are in

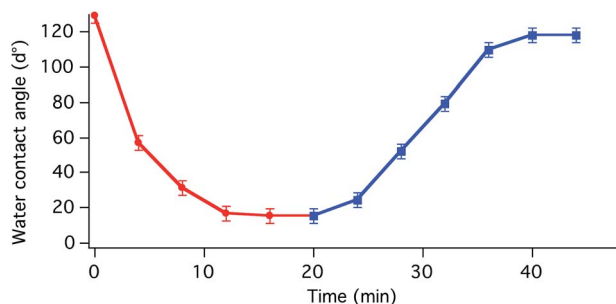


Fig. 9 Water contact angle of the 10% wt of the AzoC11 acid/TiO<sub>2</sub> film as a function of time of the UV irradiation (● in red) and time of heating at 150 °C (■ in blue).

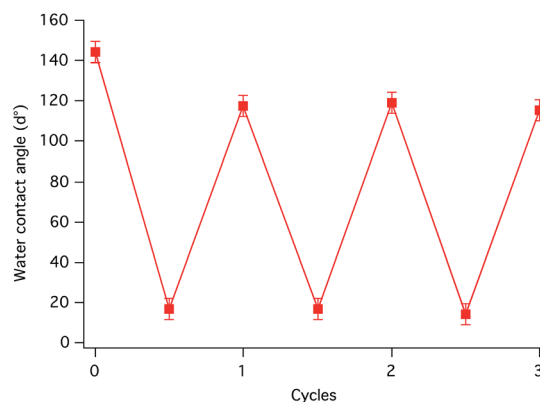


Fig. 10 Reversible wettability transition of the 10% wt AzoC11 acid/TiO<sub>2</sub> film after several cycles of 12 min UV irradiation followed by 20 min at 150 °C.

the *cis* form, the molecules may be very close against each other. Some intermolecular interactions can thus be formed<sup>61,62</sup> and can limit the *cis* → *trans* isomerization of the AzoC11 acid. To check this hypothesis, the isomerizations, *trans* → *cis* and *cis* → *trans*, of the 10% wt AzoC11 acid/TiO<sub>2</sub> film were followed by UV-vis spectroscopy in reflectance mode. The absorbance values at 438 nm (in order to avoid the TiO<sub>2</sub> absorption at 348 nm) of the 10% wt AzoC11 acid/TiO<sub>2</sub> film are reported in Table 2 after each step.

The absorption at 438 nm is characteristic of the n-π\* transition. Under UV irradiation, the absorbance at 438 nm increases, as the AzoC11 acid isomerizes from the *trans* state to the *cis* state. Also after the heating step, the absorbance at 438 nm decreases, and the AzoC11 acid returns to the *trans* state. Finally, the absorbance value after the first cycle (0.073) is very close to its initial value (0.074). It seems that the reversibility of the isomerization process in the film is satisfying, thus suggesting that the decrease of the contact angle after the first cycle (from 144° to 118°) could not stem from uncompleted *cis* → *trans* isomerisation.

The second hypothesis is based on the process related to the nature of the substrate. A decrease in contact angle after the first cycle has been already observed in the case of substrates based on TiO<sub>2</sub>,<sup>14,34,63</sup> whereas contact angles appear to be stable over the cycles in the case of silica-based substrates.<sup>64-66</sup> In the previous section we showed that the photo-generated hydroxyl groups was not the dominant process in transitions between hydrophobic and hydrophilic states. However, this process may explain the differences of the initial contact angle and the contact angle after the first cycle. Indeed, while the

Table 2 Evolution of absorbance at 438 nm of the 10% wt AzoC11 acid/TiO<sub>2</sub> film after one cycle of 12 min UV irradiation followed by 20 min at 150 °C

	Initial	After 12 min under UV irradiation	After 20 min at 150 °C
Absorbance at 438 nm	0.074	0.138	0.073

isomerization process is fast (few minutes, Fig. 9) relative to the desorption of hydroxyl groups photo-generated by UV, the return to the initial density of hydroxyl groups was shown to be very slow (several days).<sup>22,30,67</sup> Consequently, we suggest that the step at 150 °C for 20 min is not sufficient to allow a return to the initial density of hydroxyl groups. The variation of the contact angle before and after UV irradiation, reported in the literature, on the TiO<sub>2</sub> pristine are superior at 100°. <sup>22,67</sup> This assumption is supported by the estimation of the contact angle variations for a chemically heterogeneous surface by using the Cassie–Baxter law.<sup>68</sup> In the case of the 10% wt AzoC11 acid/TiO<sub>2</sub> film, the uncovered TiO<sub>2</sub> surface represents roughly 23% of the total surface, the rest of the surface being covered with the *trans*-AzoC11 acid. In this case, the contact angle variation estimated by means of the Cassie–Baxter law,<sup>69</sup> is roughly 30°, which is consistent with the experimental difference of 26° between the initial contact angle and the contact angle after the first cycle.

We finish this discussion by highlighting the dominant role of the isomerization process in variations of wetting on these hybrid materials as compared to the photo-generation of hydroxyl groups. However, the slow kinetics of desorption of these hydroxyl groups could explain the decrease in the contact angle after the first cycle.

## Conclusion

In this contribution, optimized wettability properties of a hybrid surface based on a mixture of TiO<sub>2</sub> nanoparticles with the AzoC11 acid are presented. The method used in our study allows for an easy control of the covered surface ratio of the AzoC11 acid on the TiO<sub>2</sub> nanoparticles. The maximum contact angle variations were found for a covered surface ratio of 77%.

Different processes were found to be responsible for the important changes in the contact angle. In our system, the contact angle variation induced by UV irradiation can be explained by the competition between the two mechanisms, the hydroxyl group photo-generation on the TiO<sub>2</sub> surface, and the isomerization of the azobenzene functions. This latter mechanism is preponderant, and has been demonstrated by molecular modelling to be due to two effects: (i) upon *trans* → *cis* isomerization, the dipole moment increases significantly, in turn resulting in an increase in hydrophilicity. (ii) The potential for the solvent (water) molecules to establish hydrogen bonds with the lone pairs increases in the case of the *cis*-isomer, again suggesting an increase in hydrophilicity by means of this effect.

Our hybrid surface combines the switching rapidity induced by organic surfaces and the large wetting variation observed on inorganic systems. The surface morphology exalts the wettability variation due to the presence of nanoparticles.

The main conclusion of this study is that the contact angle variations are important, reversible, and fast. The duration of a complete cycle is only 32 min. This is to our knowledge the shortest time found in the literature (Table S1 of the ESI†). While the kinetics of *cis* → *trans* isomerization is not yet fast enough to allow the integration of these materials in microfluidics devices, this study suggests these materials as good candidates for instance for self-cleaning or anti-fogging surfaces.

## Notes and references

- 1 R. Fürstner, W. Barthlott, C. Neinhuis and P. Walzel, *Langmuir*, 2005, **21**, 956–961.
- 2 L. Introzzi, J. M. Fuentes-Alventosa, C. a. Cozzolino, S. Trabattoni, S. Tavazzi, C. L. Bianchi, A. Schiraldi, L. Piergiovanni and S. Farris, *ACS Appl. Mater. Interfaces*, 2012, **4**, 3692–3700.
- 3 X. Li and J. He, *ACS Appl. Mater. Interfaces*, 2013, **5**, 5282–5290.
- 4 K. Ichimura, *Science*, 2000, **288**, 1624–1626.
- 5 A. Kausar, H. Nagano, T. Ogata, T. Nonaka and S. Kurihara, *Angew. Chem.*, 2009, **48**, 2144–2147.
- 6 D. Baigl, *Lab Chip*, 2012, **12**, 3637–3653.
- 7 R. Rosario, D. Gust, A. a. Garcia, M. Hayes, J. L. Taraci, T. Clement, J. W. Dailey and S. T. Picraux, *J. Phys. Chem. B*, 2004, **108**, 12640–12642.
- 8 D. Quéré, *Annu. Rev. Mater. Res.*, 2008, **38**, 71–99.
- 9 T. Sun, G. Wang, L. Feng, B. Liu, Y. Ma, L. Jiang and D. Zhu, *Angew. Chem.*, 2004, **43**, 357–360.
- 10 W. Yuan, G. Jiang, J. Wang, G. Wang, Y. Song and L. Jiang, *Macromolecules*, 2006, **39**, 1300–1303.
- 11 Z. Wang, L. Zhu, W. Li and H. Liu, *ACS Appl. Mater. Interfaces*, 2013, **5**, 4808–4814.
- 12 S.-S. Yoon and D.-Y. Khang, *J. Mater. Chem.*, 2012, **22**, 10625–10630.
- 13 G. B. Demirel, N. Dilsiz, M. Çakmak and T. Çaykara, *J. Mater. Chem.*, 2011, **21**, 3189–3196.
- 14 W. Sun, S. Zhou, B. You and L. Wu, *J. Mater. Chem. A*, 2013, **1**, 3146–3154.
- 15 Y. Jiang, P. Wan, M. Smet, Z. Wang and X. Zhang, *Adv. Mater.*, 2008, **20**, 1972–1977.
- 16 W. Sun, S. Zhou, B. You and L. Wu, *Macromolecules*, 2013, **46**, 7018–7026.
- 17 W. Sun, S. Zhou, B. You and L. Wu, *J. Mater. Chem. A*, 2013, **1**, 10646.
- 18 M. Chen and F. Besenbacher, *ACS Nano*, 2011, **5**, 1549–1555.
- 19 S. Patra, S. Sarkar, S. K. Bera, G. K. Paul and R. Ghosh, *J. Appl. Phys.*, 2010, **108**, 083507.
- 20 M. Miyauchi, N. Kieda, S. Hishita, T. Mitsushashi, A. Nakajima, T. Watanabe and K. Hashimoto, *Surf. Sci.*, 2002, **511**, 401–407.
- 21 R. Wang, K. Hashimoto, A. Fujishima, M. Chikuni, E. Kojima, A. Kitamura, M. Shimohigoshi and T. Watanabe, *Nature*, 1997, **388**, 431–432.
- 22 X. Feng, J. Zhai and L. Jiang, *Angew. Chem.*, 2005, **44**, 5115–5118.
- 23 H. S. Lim, D. Kwak, D. Y. Lee, S. G. Lee and K. Cho, *J. Am. Chem. Soc.*, 2007, **129**, 4128–4129.
- 24 S. Wang, Y. Song and L. Jiang, *J. Photochem. Photobiol., C*, 2007, **8**, 18–29.
- 25 N. Delorme, J.-F. Bardeau, A. Bulou and F. Poncin-Epaillard, *Langmuir*, 2005, **21**, 12278–12282.
- 26 A. Athanassiou, M. I. Lygeraki, D. Pisignano, K. Lakiotaki, M. Varda, E. Mele, C. Fotakis, R. Cingolani and S. H. Anastasiadis, *Langmuir*, 2006, **22**, 2329–2333.

- 27 L. Li, S. Pan, X. Pang, H. Chen, D. Hu, L. Ke, Y. Xiong and W. Xu, *Soft Matter*, 2012, **8**, 7357–7360.
- 28 S. Abrakhi, S. Peralta, S. Cantin, O. Fichet and D. Teyssié, *Colloid Polym. Sci.*, 2011, **290**, 423–434.
- 29 X. Pei, A. Fernandes, B. Mathy, X. Laloyaux, B. Nysten, O. Riant and A. M. Jonas, *Langmuir*, 2011, **27**, 9403–9412.
- 30 M. Han, D. Ishikawa, T. Honda, E. Ito and M. Hara, *Chem. Commun.*, 2010, **46**, 3598–3600.
- 31 S. Abrakhi, S. Peralta, O. Fichet, D. Teyssié and S. Cantin, *Langmuir*, 2013, **29**, 9499–9509.
- 32 D. Yang, M. Piech, N. S. Bell, D. Gust, S. Vail, A. a. Garcia, J. Schneider, C.-D. Park, M. a. Hayes and S. T. Picraux, *Langmuir*, 2007, **23**, 10864–10872.
- 33 H. S. Lim, J. T. Han, D. Kwak, M. Jin and K. Cho, *J. Am. Chem. Soc.*, 2006, **128**, 14458–14459.
- 34 C. Jin, R. Yan and J. Huang, *J. Mater. Chem.*, 2011, **21**, 17519–17525.
- 35 F. Su, K. Chakrabarty and R. B. Fair, *IEEE Trans. Comput. Aided Des. Integrated Circ. Syst.*, 2006, **25**, 211–223.
- 36 H. Akiyama, S. Kanazawa, Y. Okuyama, M. Yoshida, H. Kihara, H. Nagai, Y. Norikane and R. Azumi, *ACS Appl. Mater. Interfaces*, 2014, **6**, 7933–7941.
- 37 V. R. Shembekar, a. Q. Contractor, S. S. Major and S. S. Talwar, *Thin Solid Films*, 2006, **510**, 297–304.
- 38 R. Aich, F. Tran-Van, F. Goubard, L. Beouch, A. Michaleviciute, J. V. Grazulevicius, B. Ratier and C. Chevrot, *Thin Solid Films*, 2008, **516**, 7260–7265.
- 39 W. Kohn and L. J. Sham, *Phys. Rev.*, 1965, **140**, A1133–A1138.
- 40 C. Lee, W. Yang and R. G. Parr, *Phys. Rev. B: Condens. Matter Mater. Phys.*, 1988, **37**, 785–789.
- 41 A. D. Becke, *J. Chem. Phys.*, 1993, **98**, 5648–5652.
- 42 J.-D. Chai and M. Head-Gordon, *Phys. Chem. Chem. Phys.*, 2008, **10**, 6615–6620.
- 43 M. J. Frisch, G. W. Trucks, H. B. Schlegel, G. E. Scuseria, M. A. Robb, J. R. Cheeseman, G. Scalmani, V. Barone, B. Mennucci, G. A. Petersson and others, *GAUSSIAN 09 (Revision B.01)*, Gaussian, Inc., Wallingford, CT, 2009.
- 44 E. Gross and W. Kohn, *Phys. Rev. Lett.*, 1985, **55**, 2850–2852.
- 45 E. Runge and E. K. U. Gross, *Phys. Rev. Lett.*, 1984, **52**, 997–1000.
- 46 E. K. U. Gross and W. Kohn, *Density Functional Theory of Many-Fermion Systems*, Elsevier, 1990, vol. 21.
- 47 R. Bauernschmitt and R. Ahlrichs, *Chem. Phys. Lett.*, 1996, **256**, 454–464.
- 48 M. E. Casida, C. Jamorski, K. C. Casida and D. R. Salahub, *J. Chem. Phys.*, 1998, **108**, 4439–4449.
- 49 R. Dennington, T. Keith, and J. Millam, *GAUSSVIEW (Version 5)*, Semichem Inc., Shawnee Mission KS, 2009.
- 50 S. F. Boys and F. Bernardi, *Mol. Phys.*, 1970, **19**, 553–566.
- 51 Y. Zhang, P. Chen and M. Liu, *Langmuir*, 2006, **22**, 10246–10250.
- 52 When the value is superior at 100%, the term of area ratio is no longer appropriate since there is probably an AzoC11 acid overlayer on TiO<sub>2</sub>.
- 53 For the area ratio equal at 62%, the contact angle after irradiation should logically be between the contact angles of 39% and 77% of area ratios. However, this anomaly was reproducible on a large number of samples.
- 54 C. Radüge, G. Papastavrou, D. G. Kurth and H. Motschmann, *Eur. Phys. J. E: Soft Matter Biol. Phys.*, 2003, **10**, 103–114.
- 55 N. Sarkar, S. Bhatta and S. Sivaram, *Langmuir*, 1997, **13**, 4142–4149.
- 56 A. N. Shultz, W. Jang, W. M. Hetherington, D. R. Baer, L.-Q. Wang and M. H. Engelhard, *Surf. Sci.*, 1995, **339**, 114–124.
- 57 M. B. Hugenschmidt, L. Gamble and C. T. Campbell, *Surf. Sci.*, 1994, **302**, 329–340.
- 58 A. Fahmi and C. Minot, *Surf. Sci.*, 1994, **304**, 343–359.
- 59 M. Matsumoto, S. Terrettaz and H. Tachibana, *Adv. Colloid Interface Sci.*, 2000, **87**, 147–164.
- 60 To induce *cis* → *trans* isomerization on our samples, we used a thermal way, as the blue light used in solution is not enough powerful.
- 61 M. Han, T. Honda, D. Ishikawa, E. Ito, M. Hara and Y. Norikane, *J. Mater. Chem.*, 2011, **21**, 4696–4702.
- 62 D. Ishikawa, E. Ito, M. Han and M. Hara, *Langmuir*, 2013, **29**, 4622–4631.
- 63 F. V. Monteleone, G. Caputo, C. Canale, P. D. Cozzoli, R. Cingolani, D. Fragouli and A. Athanassiou, *Langmuir*, 2010, **26**, 18557–18563.
- 64 N. M. Ahmad, X. Lu and C. J. Barrett, *J. Mater. Chem.*, 2010, **20**, 244–247.
- 65 Y.-N. Zhou, J.-J. Li, Q. Zhang and Z.-H. Luo, *Langmuir*, 2014, **30**, 12236–12242.
- 66 N. Wagner and P. Theato, *Polymer*, 2014, **55**, 3436–3453.
- 67 R. Sun, A. Nakajima, A. Fujishima, T. Watanabe and K. Hashimoto, *J. Phys. Chem. B*, 2001, 1984–1990.
- 68 A. B. D. Cassie and S. Baxter, *Trans. Faraday Soc.*, 1944, **40**, 546–551.
- 69 Contact angles used in the Cassie–Baxter law for TiO<sub>2</sub> are from ref. 60.